# Engineered three-dimensional microfluidic device for interrogating cell-cell interactions in the tumor microenvironment

K. Hockemeyer,[1,2,3,4,5] C. Janetopoulos,[2,4,5,a)] A. Terekhov,[6] W. Hofmeister,[2,6,7] A. Vilgelm,[1,3] Lino Costa,[6,7] J. P. Wikswo,[2,8] and A. Richmond[1,2,3,b)]

[1]*Tennessee Valley Healthcare System, U.S. Department of Veterans Affairs, Nashville, Tennessee 37212, USA*
[2]*Vanderbilt Institute for Integrative Biosystems Research and Education, Vanderbilt University, Nashville, Tennessee 37235-1826, USA*
[3]*Department of Cancer Biology, Vanderbilt University School of Medicine, Nashville, Tennessee 37232, USA*
[4]*Department of Biological Sciences, Vanderbilt University, Nashville, Tennessee 37232, USA*
[5]*Department of Cell and Developmental Biology, Vanderbilt University, Nashville, Tennessee 37232, USA*
[6]*Center for Laser Applications, University of Tennessee Space Institute, Tullahoma, Tennessee 37388-9700, USA*
[7]*Department of Materials Science and Engineering, University of Tennessee, Knoxville, Tennessee 37996, USA*
[8]*Departments of Biomedical Engineering, Molecular Physiology and Biophysics, and Physics and Astronomy, Vanderbilt University, Nashville, Tennessee 37235, USA*

(Received 9 April 2014; accepted 4 July 2014; published online 15 July 2014)

Stromal cells in the tumor microenvironment play a key role in the metastatic properties of a tumor. It is recognized that cancer-associated fibroblasts (CAFs) and endothelial cells secrete factors capable of influencing tumor cell migration into the blood or lymphatic vessels. We developed a microfluidic device that can be used to image the interactions between stromal cells and tumor cell spheroids in a three dimensional (3D) microenvironment while enabling external control of interstitial flow at an interface, which supports endothelial cells. The apparatus couples a 200-$\mu$m channel with a semicircular well to mimic the interface of a blood vessel with the stroma, and the design allows for visualization of the interactions of interstitial flow, endothelial cells, leukocytes, and fibroblasts with the tumor cells. We observed that normal tissue-associated fibroblasts (NAFs) contribute to the "single file" pattern of migration of tumor cells from the spheroid in the 3D microenvironment. In contrast, CAFs induce a rapid dispersion of tumor cells out of the spheroid with migration into the 3D matrix. Moreover, treatment of tumor spheroid cultures with the chemokine CXCL12 mimics the effect of the CAFs, resulting in similar patterns of dispersal of the tumor cells from the spheroid. Conversely, addition of CXCL12 to co-cultures of NAFs with tumor spheroids did not mimic the effects observed with CAF co-cultures, suggesting that NAFs produce factors that stabilize the tumor spheroids to reduce their migration in response to CXCL12.  [http://dx.doi.org/10.1063/1.4890330]

## I. INTRODUCTION

While considerable progress has been made in identifying and refining hallmarks of cancer, discoveries have simultaneously highlighted the need of further exploration of the tumor

[a)]Current address: Department of Biological Sciences, University of the Sciences, Philadelphia, PA 191046.
[b)]Author to whom correspondence should be addressed. Electronic mail: ann.richmond@vanderbilt.edu

 

microenvironment (TME).[1] The TME plays a critical role in driving cancer progression, and it is now thought that the tumor evolves with its microenvironment to drive invasion and metastasis.[2,3] For example, the stroma can confer drug resistance to the tumor.[4] At all stages, the integrated cellular and structural aspects of the TME act as key mediators in what is no longer considered merely a cellular or genetic disease. The mechanisms behind this mediation, however, remain elusive, making the stromal components of the TME crucial targets for current studies.[5] Tumor cells and stromal cells release numerous growth factors, cytokines, and chemokines into the microenvironment, which combine with the mechanical features of the TME to mediate the pro- or anti-tumor influences on tumor growth and invasion. The challenge is to be able to recreate a model that captures this spatially distributed, time-dependent interacting signaling and regulatory system.

Specifically, chemokines, a family of signaling molecules and their receptors, have emerged as a means by which cellular crosstalk modulates the TME to alter its metastatic potential.[6,7] Chemokines have been shown to play an integral role in tumor pathology, particularly in breast cancer. While previously linked predominantly to inflammation, chemokines are now known to mediate angiogenesis, cellular proliferation, and recruitment of cells into the TME, namely, myeloid-derived leukocytes.[8–10] It is thus clear that these cell types and others that comprise the TME act together through chemokine-mediated signaling pathways to modulate tumor growth and metastasis. Moreover, this modulation of the TME presents an opportunity to generate an anti-metastatic phenotype.[11] These discoveries highlight the extensive potential benefits of developing a model that can be used to both study the intricacies of the human TME as well as to alter the TME to find more discriminating ways of suppressing cancer progression.

Undoubtedly, mouse models have yielded powerful insights into our understanding of cancer pathophysiology. However, the differences in cellular transformation, tumorigenesis, and metastasis between mice and humans inhibit effective translation of the knowledge gained from the mouse model to human application.[12,13] Given the substantial costs of drug development in the U.S., the value of three-dimensional (3D) *in vitro* platforms becomes more attractive. Microfluidic devices that can support 3D tissue culture are increasingly complex as there is growing recognition of both a need for the mechanical factors of the TME in addition to the commonly accepted need for a 3D cellular environment that readily mirrors the *in vivo* situation.[14–16] Recent movements toward 3D reconstituted basement membrane models have proven highly successful in reproducing the tumor phenotype *in vitro*.[17] Additionally, heterotypic cultures that incorporate endothelial cells, fibroblasts, and cancer cells (CCs), along with other stromal cells, may provide promising models for examining the TME.[18,19] Furthermore, *in vitro* models provide an opportunity to incorporate interstitial fluid pressure, as the mechanobiology of the TME has proven equally important in modulating the tumor stroma.[20–22]

We have developed a co-culture bioreactor to mimic and examine the breast cancer TME that takes into consideration the need for interstitial flow and the ability to grow numerous cell types in a 3D matrix.[23–26] This device was machined using femtosecond laser-etching technology[27,28] and mimics the TME and surrounding vasculature. The design incorporates a semicircular chamber connected to a channel 200 $\mu$m in width to an array of capillary-like channels, all machined in glass. This apparatus allows for the spatial and temporal recreation of a controlled TME *in vitro*. While a number of *in vitro* models exist for examining the tumor microenvironment, the spheroid model best recapitulates the three-dimensional tumor.[29] Thus, human microvascular endothelial cells (HMVECs), fibroblasts, and cancer cell spheroids were co-cultured within the bioreactor prior to perfusion of fluids through the channel, which was used in some experiments to generate interstitial flow. This platform is beneficial in that it can be readily modulated in real time and even modified as necessary to simulate a number of tumor microenvironments in addition to that of the breast. It moves toward a more physiologically relevant *in vitro* platform for studying the TME, and furthermore, because of the microfluidic nature of this system, this platform could be readily adapted for massively parallel testing of the potential efficacy of chemotherapeutic agents.

Using our bioreactor, we delved into the TME, focusing on cancer-associated fibroblasts (CAFs), which, in particular, have surfaced as a fundamental component of the stroma.[30] Given

their complex importance in the tumor, experiments were performed comparing spheroid sprouting *in vitro* in the presence of CAFs compared to normal tissue-associated fibroblasts (NAFs). These experiments revealed increased sprouting in the presence of cancer-associated fibroblasts, in contrast to the minimal sprouting in the presence of normal fibroblasts. MDA-MB-231 spheroids alone exhibited almost no sprouting, highlighting the importance of stromal cell presence in the TME. Cancer-associated fibroblasts are known to secrete stromal-derived factor 1, also known as SDF-1 or CXCL12, which has been shown to induce outgrowth of highly metastatic MDA-MB-231 breast cancer cells.[31] Thus, spheroids were also cultured in 10 ng/ml CXCL12 with and without normal fibroblasts. Our studies indicated that NAFs suppress spheroid sprouting, while CXCL12 and CAFs markedly up-regulate dispersion of the cancer cells out of the spheroid and invasion into the surrounding matrix. Moreover, Slit-2, a protein that binds to the Roundabout (Robo) receptor, has been shown to antagonize the migratory response of cells toward CXCL12.[32] The migratory response linked to Robo1, expressed in MDA-MB-231 cells, can be inhibited by addition of 100–250 ng/ml SLIT through abrogation of Src kinase, PI3K, MAPK, and MMP-2 and MMP9.[33] Upon examination, NAFs showed increased expression of SLIT2 and SLIT3 mRNA compared to CAFs, indicating a mechanism by which NAFs reduce MDA-MB-231 cancer cell migration in our model.

## II. METHODS

### A. Device fabrication and preparation

The experiments were conducted in a microfabricated device composed of a semicircular chamber for culture of tumor cells in 3D matrix, as shown in Figure 1. On the straight edge of the semicircle, an array of posts creates a permeable wall to contain the collagen and matrigel matrix within the culture well and supports the growth of endothelial cells in the perfused vascular compartment, as shown in Figure 1(a). Both the input and output flows in the vascular compartment were controlled independently by means of external syringe pumps connected to the fluidic channels by the inlet and outlet holes, which allowed for precise generation of interstitial flow into the semicircular chamber.

Fabrication of similar devices is described in detail elsewhere.[27,28,34] The microfluidic device was designed in AutoCAD, laser ablated with a femtosecond laser machining station, and etched in 10 M KOH solution at 80 °C for 1 h. The device was fabricated and assembled in an ISO 1000 class clean room at the Center for Laser Application of the University of Tennessee Space Institute. Two mm diameter inlet/outlet and culture-well holes were drilled through 500-$\mu$m thick fused silica wafers. One wafer was cleaved through the diameter of the well hole and half of that piece used for the semicircular culture well structure seen in Figures 1(a) and 1(e). The straight, right edge of the culture well was provided by the other wafer, whose edge presented an array of microchannels that serve as a barrier to separate the 3D matrix from the endothelial cells. At this interface, small openings of less than 6 $\mu$m wide and approximately 50 $\mu$m long were machined every 30 $\mu$m for a length of 2 mm in the area between the interstitial flow channel and the culture well of the device. The machined 500-$\mu$m thick pieces containing the well and the interstitial flow channels were then bonded to a 170-$\mu$m thick fused silica coverslip spin coated with 20 $\mu$m of polydimethylsiloxane (PDMS). The glass device was then bonded with silicone sealant to an acrylic manifold assembly that functions as a well for buffer solution and an interface to the interstitial flow and pump system. The acrylic manifold has silicone O-ring seals to the supply tubing. Interstitial flow is provided by a Harvard Apparatus Syringe Pump (Figure 1(c)).

For sterilization, the device was flushed with 70% ethanol and incubated 20 min at room temperature under a laminar flow hood. 1× PBS supplemented with 400 $\mu$g/ml penicillin, 400 $\mu$g/ml streptomycin, and 1 $\mu$g/ml amphotericin B was then flowed through the device overnight under UV light in the laminar flow hood using a. Harvard syringe pump at a flow rate of 20 $\mu$l/min. To facilitate cell adhesion, the device was coated with 200 $\mu$g/ml collagen I (high concentration, rat tail, BD Biosciences), diluted in Attachment Factor (Life Technologies) for a

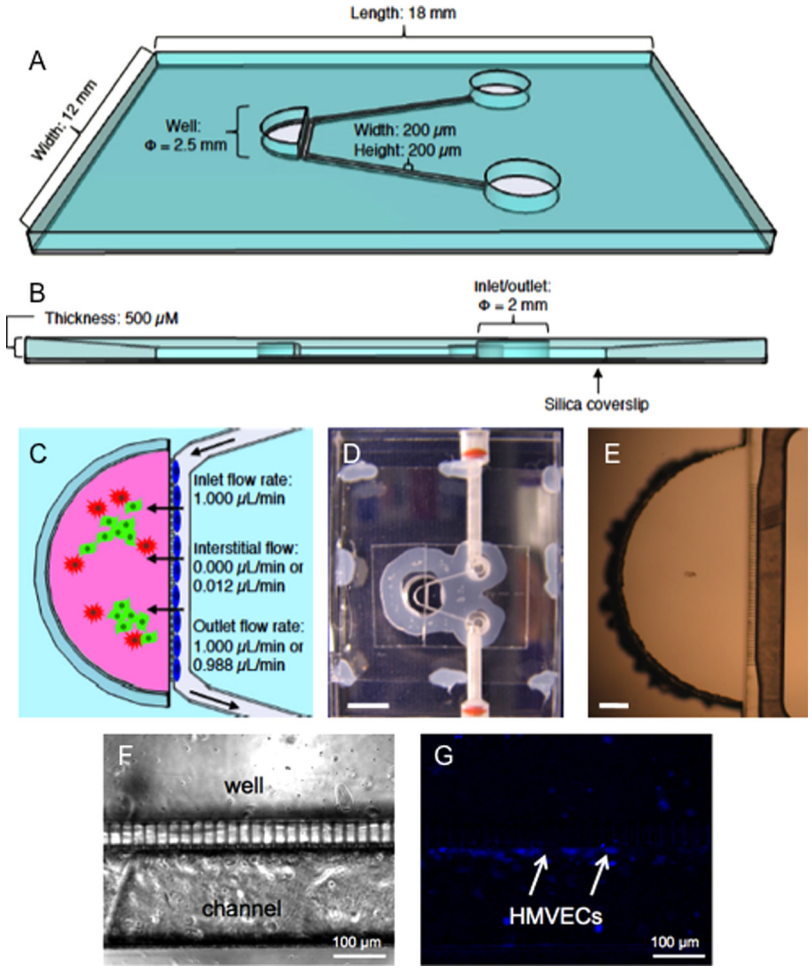


FIG. 1. Device schematic. Isometric (a) and sectional (b) views of the device etched in a silica chip and sealed to a coverslip. A zoomed in orthogonal view of the semicircular well and channel (c) displays spatial orientation of cancer cell spheroids (green), fibroblasts (red), and microvascular endothelial cells (blue) during experiment along with rates of inlet flow, outlet flow, and interstitial flow. Images of the fabricated device ((d) and (e)) give a size reference with scale bars 5 mm and 200 $\mu$m, respectively. (d) is the assembled device glued to the acrylic manifold. Inlet and outlet port supply is sealed by red o-rings on the top and bottom of the diagram. (e) A view of the cell well, interstitial flow channel and bridge between the two containing 6 $\mu$m flow channels every 30 $\mu$m. (f) A simulated vascular wall through endothelial cell monolayer is created by HMVECs labeled with Cell Tracker Blue cultured on channel side of porous membrane spatially mimic blood vessel wall. 20× magnification of channel in bright field shows some visibility of cells in monolayer. (g) 20× magnification of DAPI channel visually confirms HMVECs are beginning to form a monolayer.

minimum of 1 h at 37 °C. The semicircular chamber was coated with 0.1% poly-L-lysine solution (Sigma) for 1 h at room temperature and rinsed with PBS before use.

### B. Cell culture

All cell culture was performed using sterile technique under a Class IIA laminar flow hood. The human breast adenocarcinoma cell line, MDA-MB-231 transfected to express GFP, was cultured in Dulbecco's Modified Eagle Medium supplemented with 10% Fetal Bovine Serum (FBS) and 2 mM L-glutamine. Cancer-associated fibroblasts, bCAF33 and bCAF40T, and normal fibroblasts, hNAF112 and bNAF13, were isolated from breast cancer tissue or normal breast tissue and generously provided by the laboratory of H.L. Moses (Vanderbilt University) and the laboratory of S. Hayward (Vanderbilt University) as described by Erez.[35] Fibroblasts were cultured in MCDB-131 medium (Gibco), supplemented with 10% FBS, 1× insulin-transferrin selenium, 1× non-essential amino acids, 1.4 mM L-glutamine (Gibco), 13%

amniomax basal medium (Gibco), and 2.1% amniomax C100 supplement (Gibco). HMVECad primary cells (Life Technologies) were cultured in MCDB-131 medium supplemented with Microvascular Growth Supplement (Life Technologies).

### C. Tumor spheroid preparation

For cancer cell spheroids, MDA-MB-231-GFP cells were detached from monolayer culture with trypsin/EDTA, collected by centrifugation, and resuspended to $1 \times 10^4$ cells/ml in DMEM (10% FBS, L-glutamine) with 20% methylcellulose medium. 1000 cells were loaded into each well of a 96 well sterile non-cell-culture-treated U-bottom plate and cultured for 2–3 days to allow formation of small spheroids for use in experiments.

### D. Endothelial cell loading and culture

Endothelial cells (HMVECad) were stained with 8 $\mu$M Cell Tracker Blue in serum free MCD-131 medium for 1 h at 37 °C, followed by a 30-min incubation in culture medium not containing Cell Tracker. The cells were detached using trypsin (0.05%)/EDTA (0.53 mM) in HBSS without calcium, magnesium (Corning) added to culture medium, and centrifuged (800 g, 5 min). The cells were resuspended to a concentration of $5 \times 10^6$ cells/ml in experiment medium (culture medium buffered with 25 mM HEPES). 500 $\mu$l of experiment medium was flowed through the channel and 100 $\mu$l were added to the semicircular chamber prior to loading. The cell suspension containing endothelial cells was loaded into the device using a 100-$\mu$l gas-tight syringe and a blunt 23-gauge dispensing needle. The device was left angled for 3 h to allow the endothelial cells to seed on the interface formed by the microchannels between the perfusion channel and cell-culture well.

### E. Tumor spheroid and fibroblast loading

The GFP-MDA-231 cell spheroids were transferred to a 1.5 ml centrifuge tube using a cut pipette tip so as not to disrupt their integrity. They were washed twice with experiment medium (DMEM, 10% FBS, LG, 25 mM HEPES) and put on ice. The fibroblasts were incubated in 7 $\mu$M Cell Tracker Red for 1 h at 37 °C before detachment using TrypLE. Fibroblasts were collected by centrifugation (800 g, 2 min), suspended, counted, and aliquoted in the appropriate volume to deliver a final concentration of $2.5 \times 10^5$ cells/ml in the matrix/gel suspension. The supernatant was aspirated from the GFP-MDA-231 breast tumor spheroids and the spheroids were then aliquoted into the fibroblast cell suspension to achieve a final concentration of 50–60 spheroids in 200 $\mu$l of three-dimensional reconstituted basement membrane with 1.5 mg/ml type I collagen and 10% Matrigel.

After the endothelial cells were allowed to adhere to the device interface and form a monolayer (3 h), the semicircular chamber was loaded with 7.5 $\mu$l of the prepared gel containing Cell Tracker Red-labeled fibroblasts and GFP-labeled MDA-231 breast tumor spheroids, allowed to polymerize, and the movement of the tumor spheroids was imaged continuously over 20 h.

### F. Extracellular matrix gel preparation

The matrix/gel was prepared on ice using a 1:1 ratio of collagen solution and Matrigel solution, with a final concentration of 1.5 mg/ml collagen I (rat tail, BD Biosciences) and 10% Matrigel (BD Biosciences). The collagen was buffered with a solution of NaOH, HEPES, and 10× PBS in water. Matrigel was added, followed by cell suspension of spheroids with or without fibroblasts in experiment medium. Approximately 7.5 $\mu$l of gel was loaded into the semicircular well, and the device was incubated at 37 °C, 5% $CO_2$ for 1.5 h to allow polymerization, flipping periodically to ensure three-dimensionality of spheroid and cell distribution. 100 $\mu$l experiment medium was then added to the semicircular chamber prior to experiment. In the case of experiments with CXCL12, 100 $\mu$l of ligand diluted to 10 ng/ml in experiment medium or 100 $\mu$l vehicle solution without CXCL12, was added to the semicircular chamber after gel polymerization and prior to imaging.

### G. Microscopy and device operation

Time-lapse video microscopy was performed on a Zeiss Axiovert 200 m microscope with an incubator chamber that kept a temperature of 37 °C. The device was imaged every 15 min over 20 h under a 10× lens in bright field and for fluorescence at excitations of 488 nm and 546 nm for visualization of GFP-expressing cancer cells and fibroblasts labeled with Cell Tracker Red, respectively. Time-lapse video microscopy was performed on a Zeiss Axiovert 200 m microscope with an incubator chamber that kept a temperature of 37 °C. The device was imaged every 15 min over 20 h under a 10× lens in bright field and for fluorescence at excitations of 488 nm and 546 nm for visualization of GFP-expressing cancer cells and fibroblasts labeled with Cell Tracker Red, respectively. Individual cell migration from the spheroids was tracked using Bitplane Imaris cell tracking algorithm. Track length, track displacement, and speed were analyzed for statistical significance in Prism (GraphPad, San Diego, CA) using ANOVA.

### H. qRT-PCR analysis of Slit2, Slit3, and Robo

Total RNA was extracted from cultured CAFs, NAFs, MDA-MB-231, or co-cultures of CAFs or NAFs with MDA-MB-231 cells using RNAeasy mini kit (Qaigen) according to the manufacturer's recommendations. RNA samples were subjected to reverse transcription using iSript cDNA synthesis kit (Bio-Rad) and amplified with SYBR Select Master Mix (Life Technologies) using CFX96 Touch real-time PCR detection system (Bio-Rad). Primer sequences were SLIT3 forward CGGCATCACCGATGTGAAGAA and reverse AGGCGCAGAGTTCGGATCT; SLIT2 forward GCGAAGCTATACAGGCTTGAT and reverse TGCAGTCGAAAAGTCCTAAGTTT; ROBO1 forward GACAAAACCCTTCGGATGTCA and reverse CCAGTGGAGAGCCATCTTTCT. mRNA contents were normalized to the expression of GAPDH determined with primers forward GCCTCAAGATCATCAGCAATG and reverse CTTCCACGATACCAAAGTTGTC. For the statistical analysis of fold mRNA expression change in CAFs compared to NAFs and in CAF + CC compare to NAF + CC, a one sample T-test was performed using GraphPad Prism software and $p < 0.05$ was taken to indicate statistically significant differences.

## III. RESULTS

### A. Development of bioreactor to study the tumor microenvironment

We tested a number of reagents and procedures to determine the optimum coating of the laser etched glass that allowed the growth and adherence of endothelial cells to the machined channels, thus allowing a representation of an artificial blood vessel.[36] These reagents included poly-L-lysine, Attachment Factor (Life Technologies) supplemented with 50 $\mu$g/ml, 100 $\mu$g/ml, or 200 $\mu$g/ml collagen I (BD Biosciences), and a solution of 50 $\mu$g/ml collagen I and 0.1% acetic acid in Millipore water. After experimentation, poly-L-lysine was used to coat the well and the collagen I with acetic acid solution was used to coat the channel to improve cellular adhesion. In addition to providing a biologically relevant environment, these coatings could also be removed readily after experiment so that the device could be reused.

Human microvascular endothelial cells (200 cells in 80 nl) were cultured in the channel and made up the walls of the artificial blood vessel that was then perfused with medium. The differential between the quantity aspirated from the outlet and that perfused through the inlet could be altered by syringe pumps to generate precise interstitial flow into or out of the semicircular chamber, making this a versatile and biologically relevant model (Fig. 1). The key feature of this design is that the magnitude and direction of the interstitial flow within the 3D matrix can be adjusted, if desired, by controlling the small differential between the rate of fluid injection into the channel by one pump and the rate of fluid withdrawal by the other. Because we used volumetric syringe pumps rather than gravity feed, the interstitial flow through the matrix was controlled independent of any small changes in the perfusate level above the matrix. Hence, with equal push-pull syringe pumps on the input and output channels, this design will

insure perfusion of the endothelial cells without driving interstitial flow. This unique and innovative design also allowed *in vitro* visualization of cell migration to provide insight into the mechanisms of metastasis (Figure 1).

### B. Cancer-associated fibroblasts increase spheroid sprouting *in vitro*

Since previous studies have highlighted the influence of CAFs on the TME, experiments were performed comparing spheroid sprouting in the presence of NAFs or CAFs. Endothelial cells were cultured in the channel (shown at the arrows in Figure 1(g)), spheroids with or without CAFs were suspended in reconstituted basement membrane and loaded into the semicircular well. Imaging revealed that while in the absence of CAFs there was little dispersion of the tumor cells from the spheroid (Figure 2(a), Multimedia view), when co-cultured with CAFs there was marked dispersion of tumor cells from the spheroid along with rapid cancer cell migration when tumor spheroids were co-cultured with CAFs (Figure 2(b), Multimedia view).

### C. NAFs alter the morphology of spheroid cells but do not increase the dispersion of the MDA-231 cells from the spheroid

When experiments were performed with MDA-MB-231 spheroids in the presence of normal fibroblasts (NAFs) (Figure 2(c), Multimedia view), the cancer cells did migrate, but this movement was only in close proximity to the spheroid and there was considerably less invasion of the surrounding matrix. Of note, the spheroid cells cultured with NAFs tended to form "Single file" strings of tumor cells that did not move away from the group of GFP-tagged tumor cells.

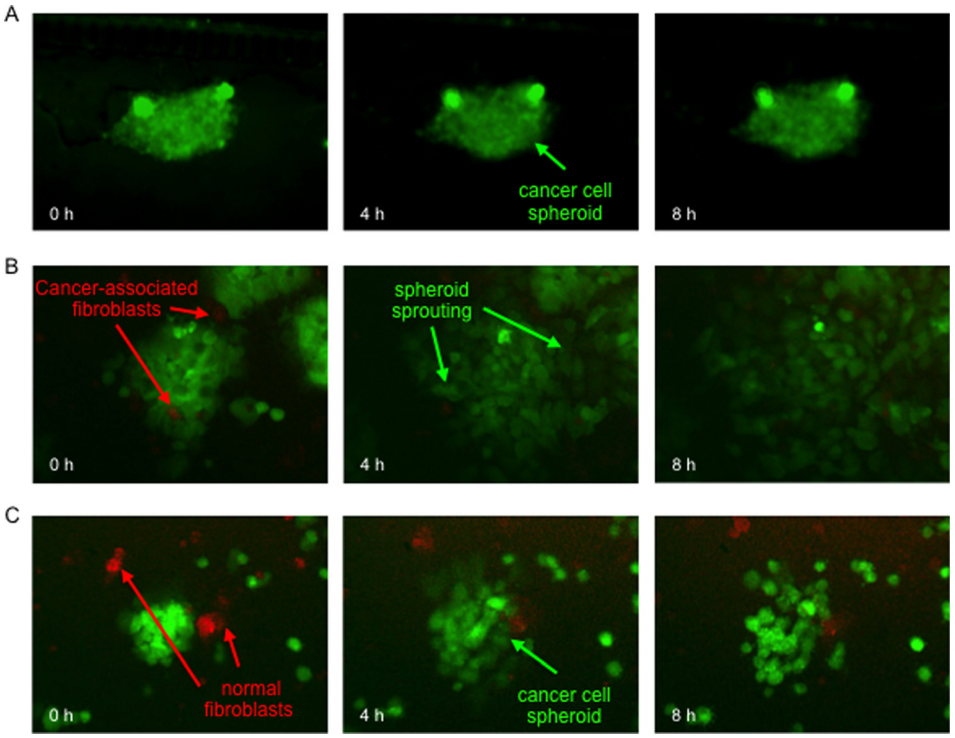


FIG. 2. Spheroid Sprouting with Spheroids Alone or in the Presence of Cancer-Associated Fibroblasts or Normal Tissue-Associated Fibroblasts. Shortly after polymerization of the reconstituted basement membrane, the device was imaged over 12 h. Cancer cells are GFP-expressing and fibroblasts were labeled with Cell Tracker Red. (a) Cancer cell spheroids alone did not exhibit sprouting. (b) Cancer cells sprouted into the surrounding matrix when cultured with CAFs. (c) When cultured with NAFs, cancer cells moved around the spheroid or within small clusters, very little migration occurred outside of local movement. (Multimedia view) [URL: http://dx.doi.org/10.1063/1.4890330.1] [URL: http://dx.doi.org/10.1063/1.4890330.2] [URL: http://dx.doi.org/10.1063/1.4890330.3]

### D. Replacement of cancer-associated fibroblasts with CXCL12 (CXCL12)

Cancer associated fibroblasts have been reported to secrete substantially elevated levels of the chemokine CXCL12 (SDF-1).[37] To evaluate whether the addition of CXCL12 could replicate the dispersion of tumor cells from the spheroid induced in response to CAFs, spheroids were incubated in the device with CXCL12 (10 ng/ml) added to the semicircular chamber to mimic the ligand in a stromally derived manner. The microfluidic device was incubated at 37 °C in the presence of 5% $CO_2$ for 20 h during which the migration of the cells was recorded using time-lapse video microscopy. Results showed that addition of CXCL12 to the spheroid cultures stimulated the migration of the CXCR4-expressing MDA-MB-231 cells in a manner very similar to that of the co-culture with CAFs (Figure 3(a), Multimedia view).

To evaluate whether addition of CXCL12 to spheroids cultured with NAFs would allow the NAFs to stimulate cancer cell dispersion from the spheroid in a manner equivalent to that of CAFs, CXCL12 (10 ng/ml) was added to the co-culture of spheroids and NAFs and the migration of the cells was followed using time-lapse video-microscopy. Results showed that addition of CXCL12 to NAF/MDA-MB-231 co-cultures induced little diffusion of tumor cells

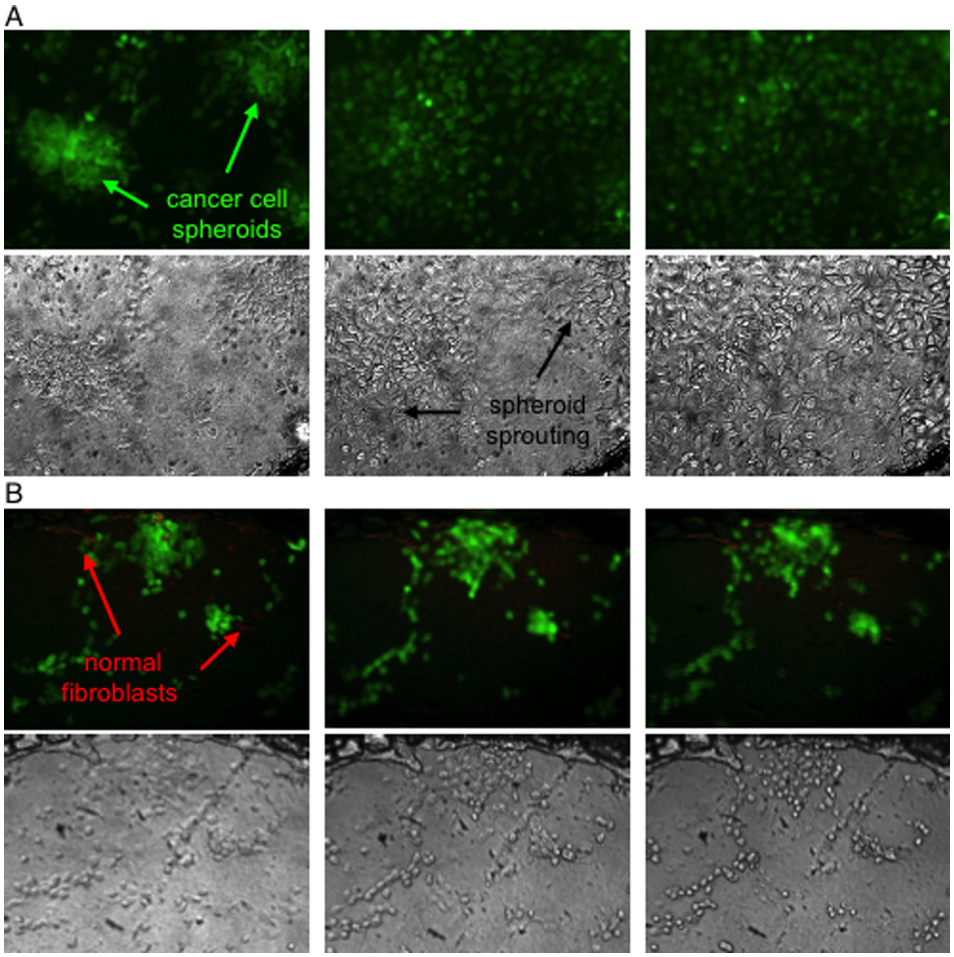


FIG. 3. Spheroid Sprouting in Response to CXCL12 (CXCL12). After polymerization, medium supplemented with 10 ng/ml CXCL12 was added to the well and the device was imaged over 20 h. (a) When stimulated with CXCL12 without the presence of fibroblasts, cancer cells sprouted extensively from the spheroid and were highly mobile within the surrounding matrix. (b) When stimulated with CXCL12 in the presence of normal fibroblasts, spheroid sprouting was abrogated and cancer cells remained localized to the spheroid. (Multimedia view) [URL: http://dx.doi.org/10.1063/1.4890330.4] [URL: http://dx.doi.org/10.1063/1.4890330.5]

from the spheroid. These data suggest that NAFs produce factors that inhibit the migration of the tumor cells in response to CXCL12 (Figure 3(b), Multimedia view).

*Quantification of time-lapse imaging data*: We performed quantitative analysis of the time-lapse imaging data using Bitplane Imaris software and also by individually tracking the migration of individual cells over time. Since some of the cells move into and out of the plane of focus, the Imaris software data were backed up with individual tracking of cells. The distance cells move varies considerably depending upon their position in the spheroid with the cells near the edge often moving a greater distance than the cells in the middle of the spheroid, resulting in rather wide standard deviations (Table I). We did observe a trend toward greater migration of cells in the spheroid in the presence of CAFs or SDF-1 as compared to the absence of either of these or in combination with NAFs. The data show there is dispersion of the spheroid in the presence of CAFs or SDF-1 (CXCL12), but not in the absence of CAFs or SDF-1, or with NAFs.

### E. Analysis of Slit2, Slit3, and Robo1 in CAFs, NAFs, and MDA-MB-231 cells and co-cultures of CAFs or NAFs with MDA-231 cells

The expression of Robo1 mRNA was not different between NAFs and CAFs or between co-cultures of NAFs and MDA-MB-231 cells versus CAFs and MDA-MB-231 cells. Interestingly, while Slit2 mRNA levels were very similar between NAFs and CAFs, when co-cultured with the MDA-MB-231 cells, the Slit2 levels in NAF co-cultures were about 2-fold higher than the CAF co-cultures. Moreover, we observed much higher levels of Slit3 mRNA in NAFs as compared to CAFs and with co-cultures of NAFs and MDA-MB-231 cells as compared to CAFs and MDA-MB-231 cells. These data suggest that when NAFs are co-cultured with MDA-MB-231 cells the inhibitory ligands, Slit2 and Slit3 are more available bind Robo1 and inhibit the migratory response to CXCL12 than in the cultures of CAFs co-cultured with MDA-MB-231 cells (Figure 4).

## IV. DISCUSSION

The microbioreactor allowed us to obtain high-resolution images of a cells migrating out from a spheroid and visualize the interactions of tumor cells in response to surrounding endothelial cells and fibroblasts in the TME. With this apparatus, there are two ways to interact with the tumor spheroids growing in the 3D matrix. Because the system is open, the 3D matrix can be manipulated through addition of reagents through the open port or through the perfusion of substances through the capillary-like channels of the machined artificial blood vessel. Furthermore, when the inlet and outlet tubings are connected to syringe pumps, the 200-$\mu$m channel is a closed system, while the semicircular chamber remains at atmospheric pressure. The inlet and outlet pressures could thus be easily altered to generate interstitial flow either into or out of the chamber. In addition to being easy to alter the environment, the easy access to the device makes it simple to clean and it can thus be reused.

As cancer-associated fibroblasts have been found to secrete CXCL12 (also known as SDF-1), experiments were performed to examine spheroid sprouting in the presence of this chemokine ligand. When treated with CXCL12, cancer cell spheroids sprouted considerably into the

TABLE I. Quantitative analysis of the time-lapse imaging data by individually tracking the migration of individual cells over time.

| Conditions | Avg migration velocity ($\mu$m/h) | Max sustained velocity ($\mu$m/h) |
|---|---|---|
| Spheroids + CAFs with Interstitial Flow | 19 | 51 |
| Spheroids + SDF1 | 18 | 46 |
| Spheroids + CAFs | 15 | 32 |
| Spheroids + NAFs | 14 | 20 |
| Spheroids + NAFs + SDF1 | 11 | 19 |

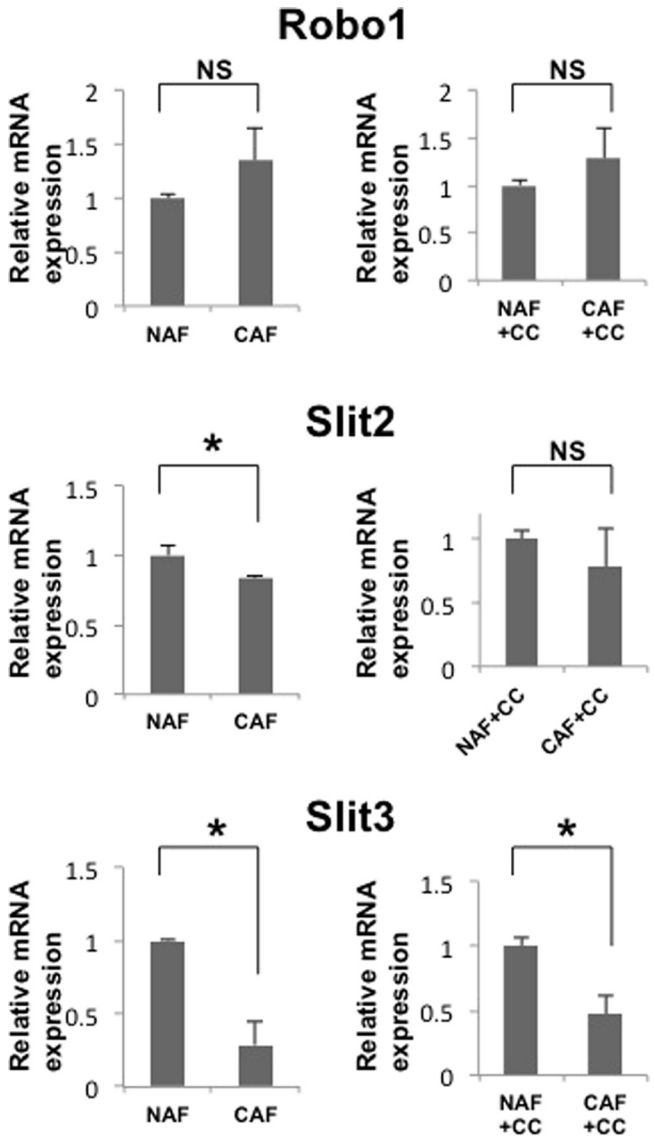


FIG. 4. Expression of Robo1 pathway genes in NAF and CAF. NAF and CAF were cultured alone or in the presence of breast CC (MDA-MB-231) for 24 h. mRNA expression levels of the indicated genes were analyzed by Real-Time PCR after reverse transcription. For the statistical analysis of fold mRNA expression change in CAF compare to NAF and in CAF + CC compare to NAF + CC, one sample T-test was performed using GraphPad Prism software. *—the fold change is significantly different from 1, $p < 0.05$. NS—not significant, $p > 0.05$.

surrounding gel (Figure 4(a)). Thus, this microfluidic device can be used to create an environment that mimics the *in vivo* situation. CAFs, but not NAFs have been shown to secrete CXCL12 and stimulate the proliferation of cancer cells and the migration of endothelial progenitor cells.[37] Zhang *et al*. recently demonstrated that when CAFs from the mesenchymal stroma of the primary tumor produce the chemokine CXCL12 (CXCL12) and the growth factor IGF1, there is selected outgrowth of a population of MDA-231 breast cancer cells that are highly metastatic. These CXCL12/IGF1 stimulated cells subsequently migrate to the bone marrow which is also rich in CXCL12 and IGF1.[31] Moreover, presence of these cytokines in the stroma selects for outgrowth of tumor cells with activated pY416-Src and inhibition of Src activity with the chemotherapeutic agent Dasatinib reduced the PI3K mediated activation or Src in the tumor cells, thus limiting the growth of the Src-hyperactive cancer cells.[31] When MDA-231 spheroids were cultured in the presence of CAFs, the MDA-231 cells rapidly disperse as

mesenchymal-like single cells out of the spheroid and into the matrix. Moreover, simple addition of CXCL12 to the spheroid cultures mimicked the addition of CAFs to the cultures of MDA-231 spheroids. These data demonstrate that the presence of the chemokine CXCL12 is a major influence on the migratory capacity of the tumor cells. Moreover, we show the utility of the microfluidic device for examining cell-cell interactions in the human TME.

Of note, this dispersion response of the MDA-231 cells in response to CXCL12 was abrogated when the spheroids were cultured with normal fibroblasts (Figure 4(b)). These experiments suggest that when the stroma surrounding the tumor is present, there may be secretion a factor (or factors) that inhibits the dispersion response to CXCL12. Since Slit-2, a protein that is expressed by stromal cells,[33] binds to the Roundabout (Robo) receptor and has been shown to antagonize the migratory response of cells toward CXCL12,[32] we examined the levels of Slit-2 and Slit-3 and Robo for Slit produced by the CAFs and NAFs alone or co-cultured with MDA-MB-231 cells by qRT-PCR. Our studies suggest a potential role for Slit3 and possibly Slit2 from NAFs in the blunted response to SDF-1 when NAFs are co-cultured with MDA-MB-231 spheroids. Thus, the microfluidic device we describe herein will be very useful for evaluating the nature of the NAF factors which suppress or enhance the migration of the tumor cells.

Interestingly, in the presence of NAFs the tumor cells that do migrate out of the spheroid do so in single file or as chains. This "Single file" migratory capacity has been previously shown to occur in breast carcinoma and ovarian cancer and some melanomas,[38] but the regulators of this type of migration remain undefined. The microfluidic device described here may be useful for exploring this regulation. Friedl and Wolf deduce that this chain migration pattern may provide cancer cells with an added ability to penetrate tissues during metastasis.[38] However, while chains formed in the presence of NAFs, the chains did not migrate substantially in the experiments observed here.

We did not observe significant collective migration, which often occurs in epithelial cancers. This type of migration is usual for metastasis through the lymphatics and it is thought to protect the migrating cells from anti-tumor leukocytes. Future experiments will utilize this device to study the influence of anti- and pro-tumor leukocytes on the tumor cell migration pattern. Leukocytes can be infused through the inlet flow tube and recirculated, allowing them to invade through the endothelial monolayer. We can then determine if they influence the migratory and survival properties of the tumor cells.

In summary, we have developed a novel microfluidic device that couples an artificial blood vessel seeded with endothelial cells and machined in glass to an *in vitro* 3-dimensional environment. This provides the opportunity for co-culture of endothelial cells, tumor cells, fibroblasts, and leukocytes in an environment that mimics many of the parameters cells are exposed to in the *in vivo* environment. The device will be very useful for evaluation of the role of stromal components on tumor cells and to test the ability of developing therapies on tumor growth, migration, and apoptosis. One of the major needs of the scientific community is the development of a protocol for studying human cells in a 3-D environment within the context of the appropriate immune and stromal cells. The device described here will be useful for answering many key questions in cancer biology. Studying tumor cells in isolation cultured on plastic and in a 2-D environment can be quite misleading, as key receptors are often not expressed in 2-D and other alterations of gene expression exist. Moreover, tumor cells need to be studied in the presence of the stromal cells they normally encounter. While immune-compromised mice are often used to analyze the growth of human tumors, this can also be misleading since the mouse stromal cells have many differences from human and the loss of important immune modulators can lead to inaccurate interpretations of response to therapies. Future studies will be directed toward including delivery of leukocytes (lymphocytes and myeloid cell populations) into the device with the appropriate interstitial flow to better mimic the human tumor microenvironment.

## ACKNOWLEDGMENTS

We thank Kevin Seale and the team in VIIBRE and SyBBURE for all their support, guidance, and encouragement. We are thankful to Hal Moses and Simon Hayward at Vanderbilt for the human

CAF and NAF cultures isolated and cultured from breast tissue. We thank Melody Swartz at the Laboratory of Lymphatic and Cancer Bioengineering, EPFL Institute, Lausanne, Switzerland for her advice and guidance in the initial development of the devices. Thanks to Tammy Sobolik and Linda Horton who provided technical support and guidance. This work was supported by grants from the TVHS and the Department of Veterans Affairs through MERIT and Senior Research Career Scientist Awards to A.R.; NIH grants R01 CA34590 (A.R.) and K12-CA90625 (A.V.); Tennessee Higher Education Commission grant to the Center for Laser Applications at UT Space Institute (W.H.); RO1GM080370 (C.J.) and Vanderbilt Discovery Award (C.J. and W.H.).

[1]D. Hanahan and R. A. Weinberg, Cell **144**(5), 646–674 (2011).
[2]K. Polyak, I. Haviv, and I. G. Campbell, Trends Genet. **25**(1), 30–38 (2009).
[3]A. R. Anderson, A. M. Weaver, P. T. Cummings, and V. Quaranta, Cell **127**(5), 905–915 (2006).
[4]E. S. Nakasone, H. A. Askautrud, T. Kees, J. H. Park, V. Plaks, A. J. Ewald, M. Fein, M. G. Rasch, Y. X. Tan, J. Qiu, J. Park, P. Sinha, M. J. Bissell, E. Frengen, Z. Werb, and M. Egeblad, Cancer Cell **21**(4), 488–503 (2012).
[5]A. Artacho-Cordon, F. Artacho-Cordon, S. Rios-Arrabal, I. Calvente, and M. I. Nunez, Cancer Biol. Ther. **13**(1), 14–24 (2012).
[6]S. Ali and G. Lazennec, Cancer Metastasis Rev. **26**(3–4), 401–420 (2007).
[7]M. O'Hayre, C. L. Salanga, T. M. Handel, and S. J. Allen, Biochem. J. **409**(3), 635–649 (2008).
[8]B. Mehrad, M. P. Keane, and R. M. Strieter, Thromb. Haemostasis **97**(5), 755–762 (2007).
[9]A. Ben-Baruch, Clin. Exp. Metastasis **25**(4), 345–356 (2008).
[10]B. Bierie, C. H. Chung, J. S. Parker, D. G. Stover, N. Cheng, A. Chytil, M. Aakre, Y. Shyr, and H. L. Moses, J. Clin. Invest. **119**(6), 1571–1582 (2009).
[11]Z. Granot, E. Henke, E. A. Comen, T. A. King, L. Norton, and R. Benezra, Cancer Cell **20**(3), 300–314 (2011).
[12]A. Rangarajan, S. J. Hong, A. Gifford, and R. A. Weinberg, Cancer Cell **6**(2), 171–183 (2004).
[13]C. E. Bryant and T. P. Monie, Open Biol. **2**(4), 120015 (2012).
[14]J. A. DiMasi, R. W. Hansen, and H. G. Grabowski, J. Health Econ. **22**(2), 151–185 (2003).
[15]J. C. Davila, R. J. Rodriguez, R. B. Melchert, and D. Acosta, Jr., Annu. Rev. Pharmacol. Toxicol. **38**, 63–96 (1998).
[16]M. A. Swartz and A. W. Lund, Nat. Rev. Cancer **12**(3), 210–219 (2012).
[17]K. J. Martin, D. R. Patrick, M. J. Bissell, and M. V. Fournier, PloS one **3**(8), e2994 (2008).
[18]T. Vargo-Gogola and J. M. Rosen, Nat. Rev. Cancer **7**(9), 659–672 (2007).
[19]S. Krause, M. V. Maffini, A. M. Soto, and C. Sonnenschein, Tissue Eng. Part C **14**(3), 261–271 (2008).
[20]J. A. Pedersen, F. Boschetti, and M. A. Swartz, J. Biomech. **40**(7), 1484–1492 (2007).
[21]T. P. Butler, F. H. Grantham, and P. M. Gullino, Cancer Res. **35**(11 Pt 1), 3084–3088 (1975).
[22]D. Fukumura and R. K. Jain, J. Cell. Biochem. **101**(4), 937–949 (2007).
[23]X. Wang, L. Sun, M. V. Maffini, A. Soto, C. Sonnenschein, and D. L. Kaplan, Biomaterials **31**(14), 3920–3929 (2010).
[24]P. Correa de Sampaio, D. Auslaender, D. Krubasik, A. V. Failla, J. N. Skepper, G. Murphy, and W. R. English, PloS one **7**(2), e30753 (2012).
[25]L. G. Griffith and M. A. Swartz, Nat. Rev. Mol. Cell Biol. **7**(3), 211–224 (2006).
[26]J. B. Kim, Semin. Cancer Biol. **15**(5), 365–377 (2005).
[27]L. Costa, A. Terekhov, D. Rajput, W. Hofmeister, D. Jowhar, G. Wright, and C. Janetopoulos, J. Laser Appl. **23**(4), 1.3614405 (2011).
[28]G. A. Wright, L. Costa, A. Terekhov, D. Jowhar, W. Hofmeister, and C. Janetopoulos, Microsc. Microanal. **18**(4), 816–828 (2012).
[29]K. M. Yamada and E. Cukierman, Cell **130**(4), 601–610 (2007).
[30]A. Ostman and M. Augsten, Current Opin. Genet. Dev. **19**(1), 67–73 (2009).
[31]X. H. Zhang, X. Jin, S. Malladi, Y. Zou, Y. H. Wen, E. Brogi, M. Smid, J. A. Foekens, and J. Massague, Cell **154**(5), 1060–1073 (2013).
[32]A. Prasad, A. Z. Fernandis, Y. Rao, and R. K. Ganju, J. Biol. Chem. **279**(10), 9115–9124 (2004).
[33]P. H. Chang, W. W. Hwang-Verslues, Y. C. Chang, C. C. Chen, M. Hsiao, Y. M. Jeng, K. J. Chang, E. Y. Lee, J. Y. Shew, and W. H. Lee, Cancer Res. **72**(18), 4652–4661 (2012).
[34]O. H. Y. Zalloum, M. Parrish, A. Terekhov, and W. Hofmeister, Rev. Sci. Instrum. **81**(5), 053906 (2010).
[35]N. Erez, M. Truitt, P. Olson, S. T. Arron, and D. Hanahan, Cancer Cell **17**(2), 135–147 (2010).
[36]F. Couet and D. Mantovani, Expert Rev. Med. Devices **9**(3), 233–239 (2012).
[37]A. Orimo, P. B. Gupta, D. C. Sgroi, F. Arenzana-Seisdedos, T. Delaunay, R. Naeem, V. J. Carey, A. L. Richardson, and R. A. Weinberg, Cell **121**(3), 335–348 (2005).
[38]P. Friedl and K. Wolf, Nat. Rev. Cancer **3**(5), 362–374 (2003).